

Time–Frequency Approaches for the Detection of Interactions and Temporal Properties in Renal Autoregulation

CHRISTOPHER G. SCULLY,¹ KIN L. SIU,² WILLIAM A. CUPPLES,³ BRANKO BRAAM,⁴ and KI H. CHON¹

¹Department of Biomedical Engineering, Worcester Polytechnic Institute, 100 Institute Road, Worcester, MA, USA; ²Departments of Anesthesiology and Medicine, David Geffen School of Medicine at University of California Los Angeles, Los Angeles, CA, USA; ³Department of Biomedical Physiology and Kinesiology, Simon Fraser University, Burnaby, BC, Canada; and ⁴Departments of Medicine and Physiology, University of Alberta, Edmonton, AB, Canada

(Received 2 April 2012; accepted 11 July 2012; published online 19 July 2012)

Associate Editor Nathalie Virag oversaw the review of this article.

Abstract—We compare the influence of time–frequency methods on analysis of time-varying renal autoregulation properties. Particularly, we examine if detection probabilities are similar for amplitude and frequency modulation for a modulated simulation signal among five time–frequency approaches, and if time-varying changes in system gain are detected using four approaches for estimating time-varying transfer functions. Detection of amplitude and frequency modulation varied among methods and was dependent upon background noise added to the simulated data. Three non-parametric time–frequency methods accurately detected modulation at low frequencies across noise levels but not high frequencies; while the converse was true for a fourth, and a fifth non-parametric approach was not capable of modulation detection. When applied to estimation of time-varying transfer functions, the parametric approach provided the most accurate estimations of system gain changes, detecting a 1 dB step increase. Application of the appropriate methods to laser Doppler recordings of cortical blood flow and arterial pressure data in anesthetized rats reaffirm the presence of time-varying dynamics in renal autoregulation. An increase in the peak system gain and detection of amplitude modulation of the Myogenic mechanism both occurred after inhibition of nitric oxide synthase, suggesting a connection between the operation of underlying regulators and system performance.

Keywords—Tubuloglomerular feedback, Myogenic response, Time–frequency analysis, Time-varying, Transfer functions, Frequency modulation, Amplitude modulation.

INTRODUCTION

Physiological systems contain time-varying dynamics which are generated by various sources including coupling between multiple interacting mechanisms and the impact of external stimuli. Such dynamics generate physiologically relevant information, and analysis of these properties can lead to new physiological and pathological insight. Renal autoregulation, the stabilization of renal blood flow (RBF) during fluctuations in blood pressure (BP), is one such phenomenon with time-varying dynamics which are largely due to two interacting systems, tubuloglomerular feedback (TGF) and the myogenic response (MR), that regulate glomerular filtration rate and prevent systemic BP fluctuations from damaging glomeruli.⁵ The MR is intrinsic to most arteriole beds and responds to local wall tension by either constricting or dilating vessels to adjust resistance which tends to stabilize RBF. In renal autoregulation, the MR occurs in the afferent arteriole and operates within a frequency range of 0.1–0.3 Hz.³⁰ TGF senses salt concentrations in the distal tubule and transfers this information through release of a mediator to the afferent arteriole, altering resistance to adjust glomerular filtration rate.¹¹ This mechanism generates limit cycle oscillations within a frequency range of 0.02–0.06 Hz. Both mechanisms act on the afferent arteriole, creating an inherent interaction between them.^{2,4,21}

The properties and effectiveness of TGF and the MR have been analyzed by monitoring the response in RBF to step changes in BP or by time-invariant frequency domain analysis, including estimation of the input/output transfer function where BP is considered the input and RBF the output.^{1,5} Use of time-invariant

Address correspondence to Ki H. Chon, Department of Biomedical Engineering, Worcester Polytechnic Institute, 100 Institute Road, Worcester, MA, USA. Electronic mail: kichon@wpi.edu

methods assumes a stationary system, but because of the need for renal autoregulation to adapt to large BP fluctuations and the interactions between the two autoregulatory mechanisms, as well as other related systems such as the renin-angiotensin system, renal autoregulation exhibits non-stationary behavior.⁶ Zou *et al.*³³ used short-time Fourier transforms (STFT) and multi-resolution Wavelet analysis to reveal non-stationary dynamics in RBF. They showed that TGF and the MR dynamics are highly time-varying, and that time-varying properties vary between normotensive and hypertensive rat models, illustrating the need for time-varying analysis to be applied in renal autoregulation studies.³³

Subsequent studies have applied a number of time-varying methods including parametric and non-parametric time–frequency representation (TFR) techniques and time-varying transfer function (TVTF) and coherence functions to renal autoregulation data.^{3,6,22,31,32} This has revealed properties such as synchronization between the TGF and MR mechanisms,^{2,24} time-varying changes in the interactions between TGF and MR,¹⁷ amplitude and frequency modulation (AM and FM, respectively) of both mechanisms,^{10,12,20,22,23} temporal variability in the system gain,³ and temporal variability in the coherence.^{31,32} In almost every study a different time-varying method was applied, adding complexity to the interpretation of results. Further, to our knowledge no direct quantitative comparison has been performed, thus, it is unknown if any one single method is the best for understanding overall dynamics of renal autoregulation or if a set of different methods is required.

The purpose of this study is to directly compare time-varying methods that have previously been applied to the study of renal autoregulation to determine if different results may be obtained that could lead to different physiological conclusions depending on the choice of method. We compare the accuracy of AM and FM detection within the TGF and MR frequency ranges using five time–frequency techniques, and we hypothesize that the variable frequency complex demodulation (VFCDM) approach provides the most accurate detection of modulation because it has previously been shown to have one of the highest resolutions when applied to renal autoregulation.²⁸ In addition, we compare 4 TVTF estimation methods to detect temporal changes in system gains, and we hypothesized that the use of a parametric modeling method would produce the most accurate gain estimates because it estimates only the most significant terms related to the renal autoregulation dynamics. We then apply the methods to analyze time-varying characteristics of renal autoregulation in anesthetized rats.

MATERIALS AND METHODS

Time–Frequency Spectral Methods

Five methods were used to estimate time-varying spectra: STFT, continuous Wavelet transform (CWT), smoothed pseudo Wigner-Ville distribution (SPWV), VFCDM, and the time-varying optimal parameter search (TVOPS) for autoregressive parameter estimation. In the following, we briefly describe each of the methods.

Short-Time Fourier Transform

The STFT is computed by using a sliding time-window and computing the Fourier transform over each section expressed as

$$\text{STFT}(t, f) = \int_{-\infty}^{\infty} x(u)h^*(u-t)e^{-i2\pi fu} du \quad (1)$$

where $x(u)$ represents the signal, $h(u-t)$ a windowing function, and $(*)$ the complex conjugate. We used a Hamming window of length 64 samples; adjusting the length of the window alters the time and frequency resolution of the STFT. This window size provided a frequency resolution small enough to detect changes in the test signal for frequency modulation.

Continuous Wavelet Transform

The CWT is computed by convolving a wavelet function with a time series as the wavelet function is dilated across scales and translated in time:

$$W(t, s) = \frac{1}{\sqrt{s}} \int_{-\infty}^{\infty} x(\tau)\psi^*\left(\frac{\tau-t}{s}\right) d\tau. \quad (2)$$

A wavelet function, ψ , is a zero-mean function that can be localized in time and space.²⁶ We used the Morlet wavelet, shown in Eq. (3). A center frequency, ω_0 , is chosen for the Morlet wavelet to set the relationship between the frequency and each scale, s . ω_0 was set to 6, similar to other groups that have used the Morlet wavelet for analyzing renal autoregulation^{10,22–24}

$$\psi(t) = \pi^{-1/4} e^{i\omega_0 t} e^{-t^2/2}. \quad (3)$$

Smoothed Pseudo Wigner-Ville

The SPWV distribution is a member of the Cohen's class of TFRs and can be obtained from a signal $x(t)$ as

$$\text{SPWV}(t, f) = \int_{-\infty}^{\infty} h(\tau) \int_{-\infty}^{\infty} g(s-t)x\left(s+\frac{\tau}{2}\right)x^*\left(s-\frac{\tau}{2}\right) \times e^{-i2\pi f\tau} ds d\tau \quad (4)$$

using a frequency smoothing window, h , and temporal smoothing window, g .⁷ In this study, we used a Hamming window for both h and g sized at 64 and 16 data points, respectively. The frequency smoothing window was set to match that used for the STFT. The temporal smoothing window, g , was set to minimize the influence of cross-terms introduced into the Wigner-Ville distribution when multiple frequencies are present in a single signal.⁷ The size of the temporal smoothing window was set as a compromise to minimize the effect of cross-terms without introducing smoothing to the point where modulation could not be recognized.

Variable Frequency Complex Demodulation

The VFCDM approach is described in detail in Wang *et al.*²⁸ It is performed in a two-step procedure as described below. The fixed-frequency approach is used to generate an initial time–frequency estimate, and the dominant frequency components in that estimate are used as backbone frequencies to generate a refined estimate using the variable frequency approach.

Fixed-Frequency Approach

Fixed-frequency complex demodulation (FFCDM) is performed by

1. The signal, $x(t)$, is multiplied by $e^{-i2\pi f_0 t}$ at a set of fixed center frequencies f_0 [0.01, 0.02... 0.49 Hz].
2. The resulting complex demodulate at each center frequency is low-pass filtered (normalized cut-off frequency of 0.01 Hz) breaking the signal into a series of band-pass filtered components.
3. The amplitude and phase of each component are determined and then used to reconstruct each component, $y(t)$, at its center frequency

$$y(t) = A(t) \cos(2\pi f_0 t + \varphi(t)). \quad (5)$$

4. The Hilbert transform is taken of each $y(t)$ to determine the instantaneous amplitude and frequency, and a TFR is constructed by combining the instantaneous amplitudes and frequencies of all components.¹⁶

Variable Frequency Approach

After FFCDM is performed to obtain an initial time–frequency estimate, the dominant frequencies are extracted as the new, now time-varying, center frequencies. VFCDM is performed by

1. The original signal, $x(t)$, is multiplied by $e^{-i \int_0^t 2\pi f_0(\tau) d\tau}$, where $f_0(\tau)$ represents the new set of time-varying center frequencies.

2. A low-pass filter (normalized cut-off frequency of 0.005 Hz) is applied to each variable frequency complex demodulate to generate a series of band-pass filtered components.
3. Amplitude and phases are determined of each component for reconstruction at the time-varying center frequency as

$$y(t) = A(t) \cos\left(\int_0^t 2\pi f_0(\tau) d\tau + \varphi(t)\right). \quad (6)$$

4. The Hilbert transform of each band-pass filtered $y(t)$ determines the instantaneous amplitude and frequency, and a refined time–frequency estimate is generated.

Time-varying Optimal Parameter Search

The TVOPS method for autoregressive parameter estimation fits the time-varying model shown in Eq. (7), where a are the AR parameters at each time index n , y is the signal, and e is the prediction error between the model and the signal. The AR parameters are estimated using TVOPS as described by Zou *et al.*³⁴ by expanding the system onto a set of basis functions. 5 Legendre basis functions and an initial AR model order of 14 were used. TVOPS is designed to select only the significant model terms from an initial over-determined model order, and has been shown to be more accurate than other model order criteria such as the Akaike Information criterion and minimum description length.¹⁸

$$y(n) = - \sum_{i=1}^P a(i, n) y(n-i) + e(n) \quad (7)$$

From the AR parameters, the time-varying spectral representation is generated as

$$S(n, f) = \frac{T}{|1 + \sum_{k=1}^m a(k, n) e^{-i2\pi f T k}|^2} \quad (8)$$

where T represents the sampling interval and m the model order.

TVTF Methods

Non-Parametric Approaches for TVTF Estimation

Four methods were used for estimating TVTF. For the non-parametric methods (FFCDM, CWT, and STFT), TVTF estimation is as follows. The time-varying spectra were computed for the input and output signals (S_X for input spectra, S_Y for output spectra) and the cross-spectrum (S_{XY}) was computed using the codrature and quadrature spectra as in

Eqs. (9) and (10). The co- and quadrature spectra were then smoothed in the temporal and frequency dimensions.²⁹ CWT spectra were smoothed with an adaptive window relative to the size of the Wavelet at each scale, as described by Torrence *et al.*²⁶ STFT and FFCDM spectra were smoothed with a boxcar window. Cross-spectra were then computed using Eq. (11), and TVTFs (H_{XY}) were computed using Eq. (12)

$$\text{CO}_{XY}(t, f) = \text{real}\{S_X(t, f)S_Y^*(t, f)\}, \quad (9)$$

$$\text{QU}_{XY}(t, f) = -\text{imag}\{S_X(t, f)S_Y^*(t, f)\}, \quad (10)$$

$$S_{XY}(t, f) = \text{CO}_{XY} - i\text{QU}_{XY}, \quad (11)$$

$$H_{XY}(t, f) = \frac{S_{XY}(t, f)}{S_X(t, f)}. \quad (12)$$

VFCDM finds the dominant components of a signal, and creates a line graph where only the most dominant frequencies are present. For transfer function analysis the goal is to understand how the input is modified at all frequencies, therefore only FFCDM was used for TVTF analysis.

Time-varying Optimal Parameter Search

The TVOPS technique for TVTF estimation is an extension of that for time–frequency spectral analysis.³² Autoregressive, a , and moving average, b , coefficients as presented in Eq. (13) are estimated using the TVOPS procedure. The TVTF gain is then determined using both sets of coefficients in Eq. (14)

$$y(n) = -\sum_{i=1}^P a(i, n)y(n-i) + \sum_{j=0}^Q b(n, j)x(n-j) + e(n), \quad (13)$$

$$H(n, f) = \frac{\sum_{j=0}^Q b(n, j)e^{-i2\pi f j}}{|1 + \sum_{k=1}^m a(k, n)e^{-i2\pi f k}|^2}. \quad (14)$$

Test Signals

Comparative Test for Frequency and Amplitude Modulation

Two test signals were designed to test the detection of AM and FM sequences present in renal autoregulation using the time–frequency methods. The first test signal, shown in Eq. (15), contains a low frequency (LF) component at 0.025 Hz, representative of TGF, and a high frequency (HF) component at 0.16 Hz, representative of the MR, which are both constant in amplitude and frequency over 1000 s

$$y(t) = \sin(2\pi * 0.025 * t) + \sin(2\pi * 0.16 * t). \quad (15)$$

This signal was designed to determine a significance threshold for when AM or FM do not exist but may be mistakenly identified by either an influence of the time–frequency method or the background noise. 1000 realizations of Gaussian white noise (GWN) were added to the signal at signal-noise ratios (SNR) of 0 to 10 dB, in 1 dB increments. For each of the 1000 realizations at each noise level, the TFR was generated for the five time–frequency methods and a threshold was determined for significant modulation for each time–frequency method. From each TFR, the maximum amplitude and corresponding frequency at each time instant were extracted within the TGF (0.02–0.06 Hz) and MR (0.1–0.3 Hz) frequency ranges. These constituted the LF and HF AM and FM sequences. Next, the fast Fourier transform (FFT) was computed for each sequence. Statistical thresholds were computed for each of the four sequences (LF-AM, LF-FM, HF-AM, HF-FM), as well as for each noise level, as the mean plus two standard deviations of the FFT magnitudes at each frequency over the 1000 realizations.

The second test signal was designed to test if the methods detect AM and FM when it exists. This signal contains an LF component at 0.025 Hz and an HF component at 0.16 Hz. The LF component contains AM and FM at a frequency of 0.01 Hz, a frequency previously identified in renal autoregulation.^{9,20} The HF component contains AM and FM at 0.025 Hz, representing the interaction previously shown between TGF and the MR.²² The expression for the second test signal and corresponding AM and FM components are shown in Eqs. (16a)–(16e)

$$y(t) = (1 + \text{AM}_{\text{LF}}(t)) * \sin(2\pi * 0.025 * t + \text{FM}_{\text{LF}}(t)) + \dots (1 + \text{AM}_{\text{HF}}(t)) * \sin(2\pi * 0.16 * t + \text{FM}_{\text{HF}}(t)) \quad (16a)$$

$$\text{AM}_{\text{LF}}(t) = 0.25 * \sin(2\pi * 0.01 * t), \quad (16b)$$

$$\text{AM}_{\text{HF}}(t) = 0.5 * \sin(2\pi * 0.025 * t), \quad (16c)$$

$$\text{FM}_{\text{LF}}(t) = 2\pi * 0.005 * \int_0^t \sin(2\pi * 0.01 * \tau) d\tau, \quad (16d)$$

$$\text{FM}_{\text{HF}}(t) = 2\pi * 0.025 * \int_0^t \sin(2\pi * 0.025 * \tau) d\tau. \quad (16e)$$

GWN was added to the test signal at SNRs from 0 to 10 dB, in 1 dB increments. The TFRs were generated using each of the 5 methods, and AM and FM

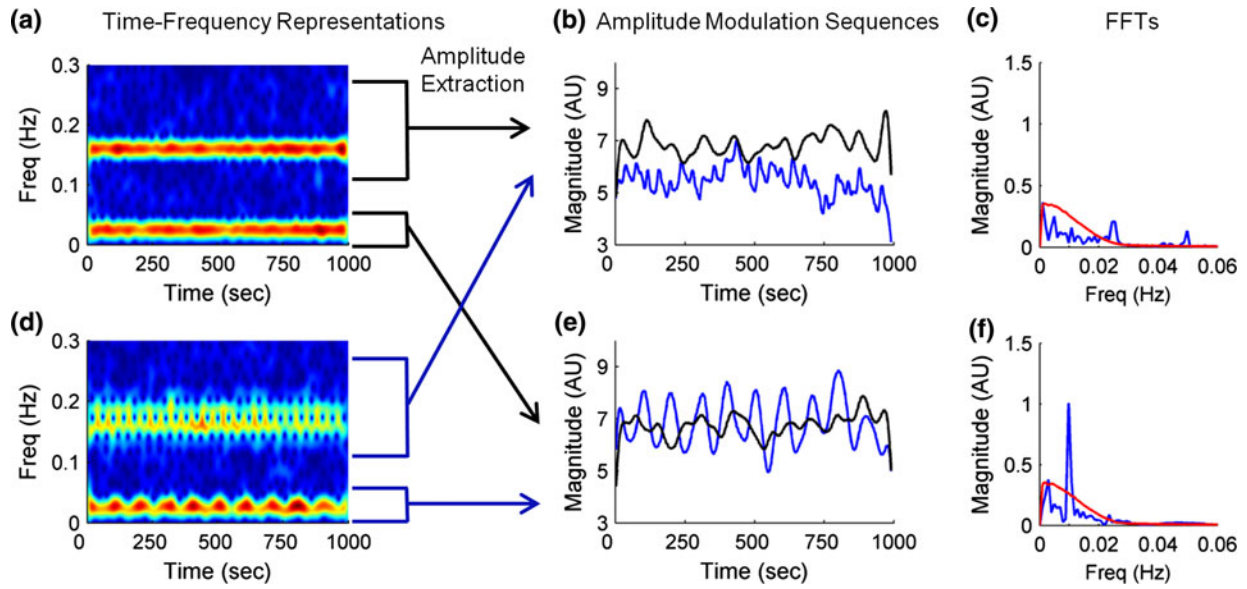


FIGURE 1. Procedure for detection of amplitude and frequency modulation. (a) The short-time Fourier transform (STFT) of the non-modulated test signal with GWN added at a signal to noise ratio of 10 dB, the signal contains stationary amplitude and frequency components over time and (d) the STFT of the modulated test signal with GWN containing high and low frequency components both with amplitude and frequency modulation. (b) Extracted amplitude sequences from the high frequency region for the non-modulated (black) and modulated (blue) signals. (e) Extracted amplitude sequences from the low frequency region for the non-modulated (black) and modulated (blue) signals. (c) FFT of high frequency amplitude sequence for modulated test signal (blue). Spectral peak at 0.025 Hz on blue represents the frequency of amplitude modulation. For comparison, the high frequency amplitude modulation threshold derived from the non-modulated signal using the STFT with GWN added to the non-modulated signal for 1000 realizations is shown (red). (f) FFT of low frequency amplitude sequence for modulated test signal (blue). Spectral peak at 0.01 Hz on blue represents the frequency of amplitude modulation for the low frequency component. The threshold derived for the low frequency amplitude modulation is shown (red). The frequency corresponding to the maximum amplitude for the low and high frequency components at each time point is also extracted and the FFT of that sequence is used to determine if frequency modulation exists. This procedure is repeated for each time–frequency representation at SNRs from 0 to 10 dB.

sequences were extracted as described above for the non-modulated signal. The modulation frequency was found as the peak FFT magnitude within the frequency ranges of 0.005–0.02 Hz for the LF sequences and 0.005–0.06 Hz for the HF sequences. Modulation peaks were considered significant if greater than the threshold derived from the non-modulated test signal. This statistical test fixes the probability of detecting a false positive (detecting modulation for a non-modulated signal) at 5%.

If significant modulation was found within the modulated test signal at a frequency within ± 0.0025 Hz of the set modulation frequency in (16) a true positive was declared, otherwise a missed detection was declared. The probabilities of detecting a true-positive (P_D) were computed for each time–frequency method for AM_{LF} , FM_{LF} , AM_{HF} , and FM_{HF} over 1000 realizations at each noise level. An example of the test for the detection of modulation is shown in Fig. 1.

Comparative Test for Identifying Time-Varying Changes in System Gain

A transfer function, represented by the z -transform $H(z)$ in Eq. (17), was designed with an LF (0.04 Hz) and HF (0.18 Hz) peak to represent TGF and the MR,

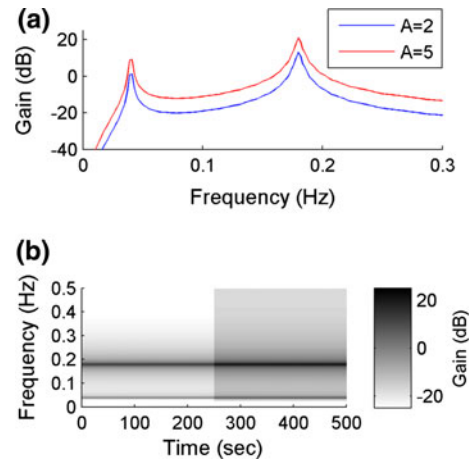


FIGURE 2. (a) Frequency response of the transfer function, $H(z)$, in Eq. (17) for two different values of the gain parameter A . (b) Time-varying transfer function generated by increasing A at 250 s.

respectively. The parameter A is used to adjust the system gain, shown by the frequency response in Fig. 2a

$$H(z) = A \frac{0.0496z^{-1} - 0.1206z^{-2} + 0.0923z^{-3} - 0.0213z^{-4}}{1 - 2.774z^{-1} + 3.6z^{-2} - 2.727z^{-3} + 0.9727z^{-4}}. \quad (17)$$

A 500 s TVTF was generated by setting a step increase in A at 250 s, as shown in Fig. 2b. TVTFs were designed so that the step increase in gain ranged from 0 to 8 dB in 1 dB increments. TVTFs were estimated from 1000 output sequences generated from Eq. (17) with 1000 realizations of GWN as the input. The maximum gain within the LF (0.02–0.06 Hz) and HF (0.1–0.3 Hz) regions were extracted at each time point for each TVTF estimate. A t test was performed to determine if the gain increase was significant ($p < 0.05$) between the first and last 250 s. The probability of detecting the change in gain at each step increase was then determined over the 1000 estimates for each of the four methods.

Renal Autoregulation Data

All experiments were performed at the State University of New York at Stony Brook and approved by the Institutional Research Board (IACUC). Sprague-Dawley rats (SDR, $n = 7$) and spontaneously hypertensive rats (SHR, $n = 7$) were anesthetized with isoflurane (3% initial, 1% maintenance), and then placed on a temperature controlled surgical table to maintain body temperature at 37 °C. The left femoral artery was catheterized for measurement of arterial pressure and the left femoral vein was catheterized for saline infusion (PE-50 and PE-10 tubing). The left kidney was isolated and placed in a Lucite cup with a thin plastic film covering the cortical surface to prevent evaporation. A supra-renal aortic clamp was used to control renal perfusion pressure. A laser-Doppler instrument (Transonic, Ithaca, NY) was used to monitor cortical blood flow (CBF) with a blunt 11-gauge needle probe placed on the cortical surface. CBF and BP were recorded continuously during the following protocol: (1) 3–5 min spontaneous BP, (2) renal arterial pressure was reduced by 20–30 mmHg below spontaneous BP by adjusting the aortic clamp, (3) CBF was allowed to stabilize at the reduced BP (approximately 1 min) and then the clamp was quickly released, (4) CBF and BP were monitored for an additional 3–5 min. N^{ω} -nitro-L-arginine methyl ester (L-NAME, Sigma-Aldrich) at 5 mg/kg body weight in 5 mL normal saline was continuously infused for 1 h, after which the protocol measurements were repeated with L-NAME present.

CBF and BP data were recorded at 100 Hz (Powerlab, ADInstruments, Mountain View, CA). Data were low-pass filtered with a cutoff frequency of 0.5 Hz to avoid aliasing, and then down-sampled to 1 Hz. Time–frequency spectral (CBF signal) and TVTF (BP as the input signal and CBF as the output signal) methods were applied to the recordings from

the entire monitoring protocol after removal of the linear trend. The maximum spectral amplitude and corresponding frequency were extracted for AM and FM detection after release of the aortic clamp from the TFRs for the MR frequencies. Modulation of TGF was not examined due to the 3–5 min data length. The maximum gain from the TVTFs was extracted from the 50 s time point after release of the aortic clamp for the TGF and MR frequencies.

A statistical threshold for modulation was derived for each CBF signal. The SNR for the TGF and Myogenic peaks were determined for each signal from the power spectral density. The TGF power within the range of 0.02–0.05 Hz was compared with the power in the assumed TGF noise region of 0.05–0.08 Hz, and the Myogenic power within the range of 0.1–0.3 Hz was compared with the power in the assumed Myogenic noise region of 0.3–0.5 Hz. A test signal was generated as the sum of two non-modulated sinusoids at the peak TGF and Myogenic frequencies with added GWN and a length equal to that of the data. The power of the TGF and Myogenic peaks relative to the GWN was set to equal the SNR of the data. 1000 realizations of this signal were generated, and a significance threshold was determined for the mean plus two standard deviations of the FFT of the AM and FM sequences extracted from the TFR's for both frequency ranges. This method tests for modulation in the data compared to a signal without modulation but with the same frequencies, SNR, and data length of the data.

Statistics

Statistical analysis was performed with SigmaStat 3.5 (Systat Software Inc.) with $p < 0.05$ considered significant. Renal autoregulation parameters were determined to be non-Gaussian using the Kolmogorov-Smirnov test. Extracted renal autoregulation parameters from after release of the clamp were compared using either the non-parametric Rank Sum test (SDR baseline vs. SHR baseline) or Signed Rank test (SDR baseline vs. SDR during L-NAME). Spearman Rank Order correlation coefficients were used to compare estimated gains between methods.

RESULTS

Comparison of Methods with Test Signals

Test for Amplitude and Frequency Modulation

Example time–frequency spectra for the modulated signal with added GWN (SNR of 8 dB) for the five methods are shown in Fig. 3. Only the first 500 s of the spectra are shown for visualization. Not all methods

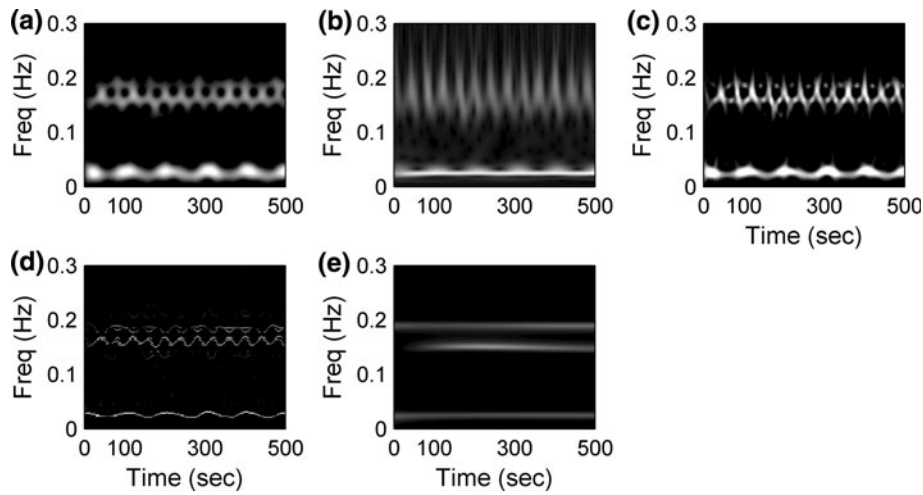


FIGURE 3. Example time–frequency representations of the modulated test signal with added noise (signal-noise ratio of 8 dB). (a) Short-time Fourier transform, (b) Wavelet transform, (c) smoothed pseudo-Wigner-Ville distribution, (d) variable frequency complex demodulation, (e) time-varying optimal parameter search autoregressive method.

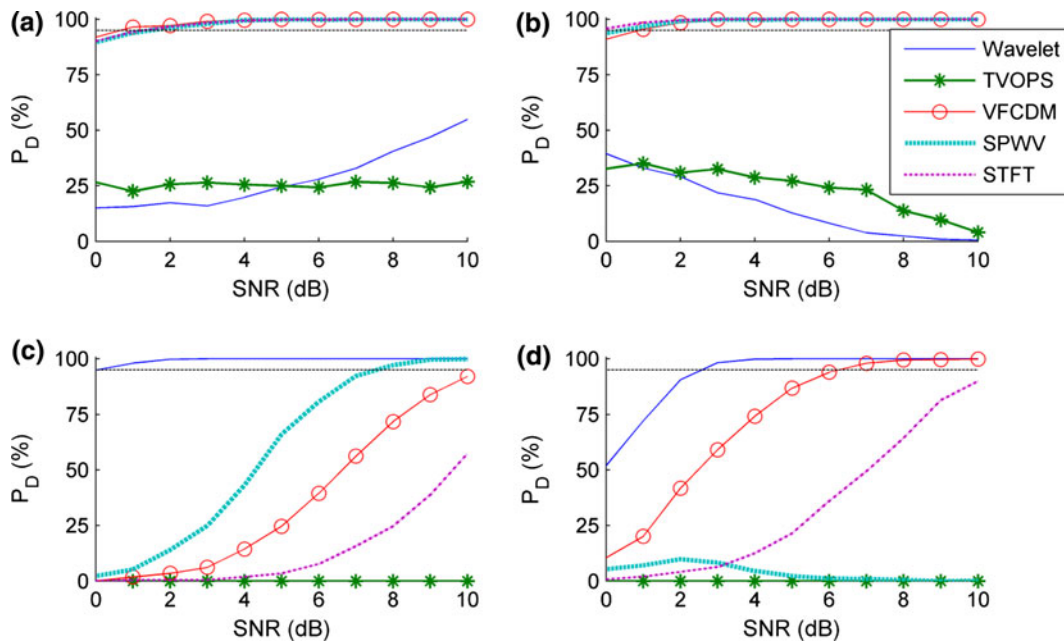


FIGURE 4. Probability of detection (P_D) for amplitude or frequency modulation in the simulation signal compared to the threshold levels at signal to noise ratios (SNR) from 0 to 10 dB for five time–frequency methods. (a) Amplitude modulation in the low frequency range, (b) frequency modulation in the low frequency range, (c) amplitude modulation in the high frequency range, (d) frequency modulation in the high frequency range. The dashed black line represents the 95% detection level.

are able to identify modulation at both LF and HF. Figure 4 shows the detection probabilities for the modulated test signal at SNRs from 0 to 10 dB. VFCDM, STFT, and SPWV methods had high levels of detection for AM and FM within the LF region across all noise levels. The CWT approach had high detection of modulation within the HF region for low SNR, but the VFCDM method also approached high detection at higher SNR. The TVOPS parametric

approach did not accurately identify modulation at any noise level.

Test for Time-Varying System Gain

Examples of the extracted LF and HF gains averaged over 1000 realizations are shown in Figs. 5a and 5c, respectively, for the estimated TVTFs for an 8 dB step increase in gain at 250 s. TVOPS accurately

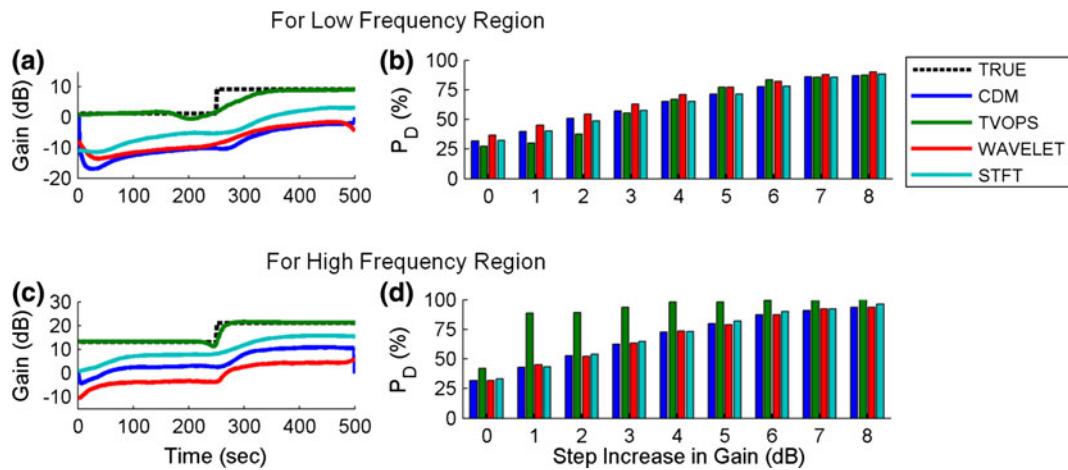


FIGURE 5. Estimated maximum gains within the low frequency (a) and high frequency (c) regions using the 4 time-varying transfer function methods (mean of 1000 realizations). (b) Probability of detecting the step increases in gain for the low frequency component over 1000 realizations of GWN. (d) Probability of detecting the step increases in gain for the high frequency components.

estimates the correct gain, while the non-parametric methods underestimate the maximum gain. P_D s for each step increase in gain determined from the 1000 realizations are presented for the LF and HF gains in Figs. 5b and 5d, respectively. In the LF range, the four methods have approximately the same P_D at each gain increase. For the HF range, TVOPS had higher P_D than the non-parametric approaches at each step increase in gain.

Application to Renal Autoregulation

Detection of Amplitude and Frequency Modulation in Renal Cortical Blood Flow

Figure 6a shows a typical low-pass filtered and down-sampled laser Doppler CBF and arterial BP signal recorded for an SDR after infusion of L-NAME, and the corresponding TFR generated with the VFCDM is shown in Fig. 6b. CBF signals were tested for AM and FM after release of the aortic clamp for the SDR and SHR animals before (baseline) and during L-NAME. Because our simulations showed that only the Wavelet and VFCDM methods reliably detect AM and FM in the MR range, we only present the results for those two methods. The number of signals detected to contain modulation out of the total number tested (7) is shown in Fig. 7a for AM and Fig. 7c for FM. The frequency at which modulation was detected is presented in Figs. 7b and 7d for AM and FM, respectively. AM of the MR was detected during baseline for 4 animals using CWT but was not detected using VFCDM. During L-NAME, modulation was detected for all 7 SDR and 5 out of 7 SHR animals, for both methods. This is in accordance with our simulation results where it was shown that wavelets had better detection within the HF region at low SNR. The

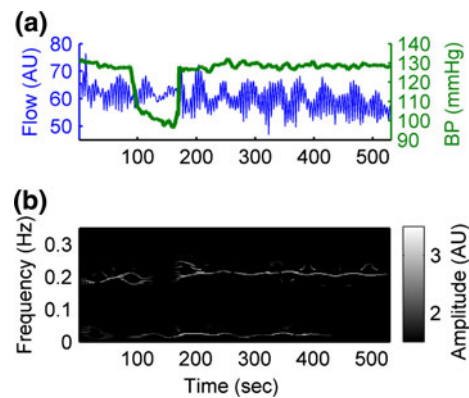


FIGURE 6. (a) Example renal data from laser Doppler flow probe (blue) and arterial blood pressure (green) obtained during renal clamping experiment from a Sprague-Dawley rat during infusion of L-NAME. Blood pressure is clamped at approximately 90 s and held for approximately 90 s after which the clamp is released. (b) Time-frequency plot generated using variable frequency complex demodulation for flow data in (a) showing the two renal autoregulation dynamics. The myogenic response occurs at approximately 0.2 Hz and TGF occurs at approximately 0.05 Hz.

frequency of significant AM ranged from 0.0078 to 0.0244 Hz using CWT and 0.0078–0.0498 Hz using VFCDM for SDR, but was limited to 0.0098–0.0137 Hz for SHR using both CWT and VFCDM. FM of the MR was detected using either approach, and the frequency detected depended partly upon the approach used. CWT showed FM at higher frequencies (0.0088–0.0352 Hz) than VFCDM (0.0078–0.0205 Hz) during L-NAME.

Transfer Function Analysis of Renal Blood Flow and Blood Pressure

Examples of the estimated TVTFs from the BP and CBF data in Fig. 6a are shown in Fig. 8. A peak gain

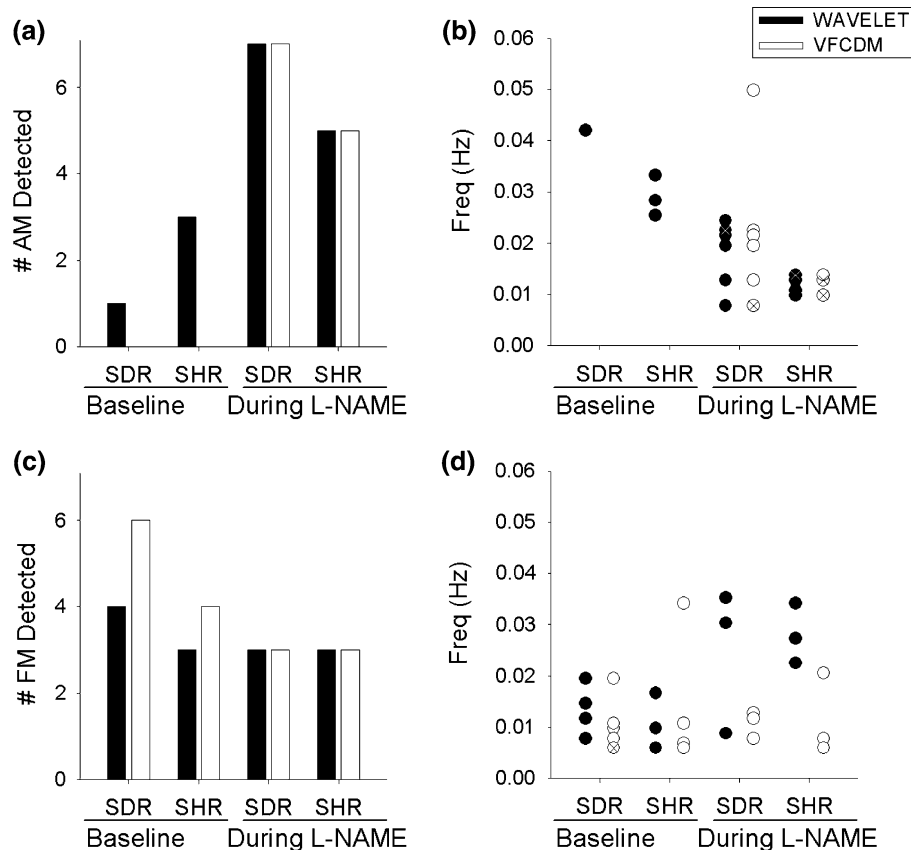


FIGURE 7. (a) Number of experiments with significant myogenic amplitude modulation (out of 7) for SDR and SHR rats after release of the pressure clamp during the baseline condition and during L-NAME. Results are shown for detection with Wavelet (black) and variable frequency complex demodulation (white) time–frequency methods. (b) Frequency at which myogenic amplitude modulation is detected for significant experiments in (a). Each circle represents an animal with significant modulation at that frequency, and an ‘x’ through the circle represents two animals with significant modulation at that frequency. (c) Number of experiments with significant myogenic frequency modulation. (d) Frequency at which the frequency is being modulated at for significant experiments in (c).

at ~ 0.2 Hz can be visualized for all four methods corresponding to an MR peak. The TGF peak (~ 0.05 Hz) strengthens after release of the aortic clamp. The median and ranges of the gains after release of the aortic clamp using each of the four methods are shown in Table 1. Gain of the MR significantly increased during L-NAME in the SDR group, determined by each of the four methods. The MR gain for SHRs was not significantly different than the SDR gain during baseline for any of the four methods, consistent with previous results.²⁷ For TGF, SDR gain significantly decreased using the FFCDM method during L-NAME, but was not significantly different using any of the other TVTF methods. SHR animals had significantly reduced TGF peak gain determined by the FFCDM, CWT, and STFT methods, but not TVOPS. Spearman Rank Order correlation coefficients estimated for the MR and TGF gains between each pair of methods, Table 2, demonstrate that changes in gain are in accordance between the various methods.

DISCUSSION

In this study, we investigated analytical methods used for monitoring time-varying renal autoregulation dynamics. Our modulation and time-varying gain tests complement each other in that one is looking for the interaction between autoregulation components² and the other is looking at how the system responds to changes in BP.³ By detecting multiple properties from the signals we can develop a better understanding of the physical regulation, and in turn how this changes the overall effectiveness of the system. Our test for AM and FM detection showed the VFCDM, STFT, and SPWV to have high P_D across noise levels in the LF range, and Wavelet analysis showed the best detection in the HF range across noise levels. The VFCDM produced the best combination of AM and FM detection in the low and HF regions. Our test for detecting time-varying changes in system gain showed that the TVOPS estimation technique detected a step

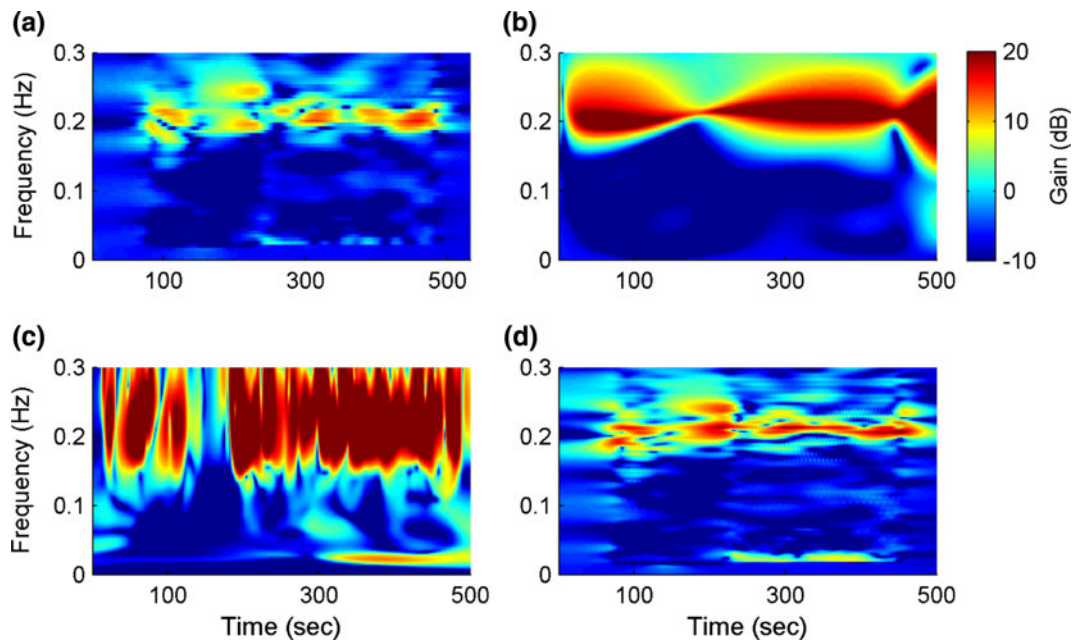


FIGURE 8. Time-varying transfer functions of laser Doppler flow and arterial pressure data shown in Fig. 6a. (a) Fixed-frequency complex demodulation, (b) time-varying optimal parameter search, (c) Wavelet transform, (d) short-time Fourier transform.

TABLE 1. Estimated transfer function gains (dB) (median, min-max) after release of the clamp for the myogenic and TGF components during baseline and with L-NAME infused.

	FFCDM	TVOPS	Wavelet	STFT
Myogenic				
SDR—baseline ($n = 7$)	1.2 -1.6 to 3.5	2.7 -1.7 to 5.7	3.4 -1.9 to 4.7	4.3 0.3-6.1
SDR—during L-NAME ($n = 7$)	8.8 ^α 1.9-11.6	16.5 ^α 12.0-33.7	19.0 ^α 8.6-26.1	13.5 ^α 6.2-15.8
SHR—baseline ($n = 7$)	-0.05 -2.0 to 2.2	2.89 -2.0 to 17.0	0.78 -1.1 to 17.0	2.9 0.1-7.3
Tubuloglomerular feedback				
SDR—baseline ($n = 7$)	-2.7 -4.8 to 0.1	-6.6 -10.0 to 1.7	-2.3 -8.6 to 4.2	-0.6 -4.8 to 2.4
SDR—during L-NAME ($n = 7$)	-4.6 ^α -8.3 to -1.4	-6.74 -14.0 to -5.8	1.1 -12.9 to 8.8	-0.9 -8.9 to 4.6
SHR—baseline ($n = 7$)	-5.5 ^α -8.4 to 0.2	-8.5 -12.1 to 0.6	-5.2 ^α -9.7 to -2.7	-5.4 ^α -8.5 to 0.2

α denotes significance from SDR during baseline conditions, $p < 0.05$.

TABLE 2. Spearman Rank Order correlation coefficients between the methods for the estimated transfer function peak gains after release of the clamp.

	CDM	TVOPS	Wavelet	STFT
CDM		0.61^α	0.76^α	0.95^α
TVOPS	<i>0.41</i>		0.83^α	0.75^α
Wavelet	<i>0.46^α</i>	<i>0.54^α</i>		0.85^α
STFT	<i>0.81^α</i>	<i>0.50^α</i>	<i>0.82^α</i>	

The upper triangle (bold entries) contains the coefficients for the myogenic range, and the lower triangle (italic entries) contains the coefficients for the TGF range. α signifies that the correlation coefficient is significant, $p < 0.05$.

increase in gain within the HF region better than the non-parametric methods. These results demonstrate that to fully characterize renal autoregulation a variety of analysis techniques with parameters tuned to the specific component of interest should be used.

We used the same time-frequency analysis parameters for analyzing the MR and TGF frequency ranges. All four non-parametric methods (STFT, CWT, SPWV, and VFCDM) identified AM and FM in at least the TGF or MR region for the simulated signals. The difference in the results between the two frequency regions is a function of the selection of the time- and

frequency-window settings for each method. For example, by varying the initial parameters that determine the frequency resolution it is possible to alter each method to better identify modulation in the MR and TGF frequency regions. This also implies that using the same parameters for both frequency regions may not be always appropriate. A window containing more samples is required to analyze the TGF than the MR dynamic because TGF operates at a slower frequency. For a window of any given size, more oscillations from the MR will be captured than TGF (since the former has faster frequency dynamics than the latter) and therefore temporal changes will be smoothed at a different rate relative to the oscillation for the two components. Wavelet methods adjust the frequency resolution based on the frequency being analyzed but concomitantly adjust the temporal resolution. Hence, the Wavelet temporal resolution within the TGF region was not sufficient to identify the temporal changes in the simulated TGF dynamics caused by modulation at 0.01 Hz.

For the SPWV, an AM sequence occurred at an incorrect frequency for the HF region during the modulation test. This resulted in poor detection of the true AM sequence and may be a function of cross terms that exist from the estimation of the SPWV distribution. Increasing the length of the temporal smoothing window will decrease these cross terms but also decrease detection of temporal changes such as modulation. This results in a trade-off between artifacts generated by cross terms and loss of information due to smoothing.⁷ TVOPS was not able to resolve the modulation in the spectral analysis because of an insufficient model order. The model order was selected based on optimization for the TVTF analysis, where the TVOPS showed the most accurate results, and was kept constant for the modulation test to show the necessity of selecting the model order based on a particular analysis.

Siu *et al.*²⁰ used a VFCDM based AM/FM detection procedure to find significant MR modulation by a 0.01 Hz frequency in whole kidney blood flow during telemetric recordings. Sosnovtseva *et al.* used a double Wavelet approach to monitor modulation in tubular pressure of single nephrons, and they initially showed that the MR was modulated by TGF.^{10,22,23} Later, it was shown that the MR could be modulated by both TGF and a 0.01 Hz frequency.¹² In the present study, we looked for modulation of the MR from 0.005 to 0.06 Hz. We found that the dominant frequency of modulation of MR can range from 0.01 to 0.06 Hz, agreeing with the study by Pavlov *et al.* that the MR amplitude and frequency may be modulated by either a 0.01 Hz mechanism or TGF.¹²

Many factors influence the dynamics of renal autoregulation, including nitric oxide (NO).⁵ NO is a

vasodilator synthesized by nitric oxide synthase (NOS) from its precursor L-arginine. It plays an important role in regulating glomerular capillary pressure, glomerular plasma flow, and TGF.⁵ The role of NO in the control of renal afferent arteriole resistance was studied by Pittner *et al.*¹⁵ using the isolated perfused rat kidney. The afferent arteriole did not autoregulate during the cell-free perfusion of the kidney, however, it did during cell-free perfusion with L-NAME.¹⁵ These results suggest that NO release is related to impaired autoregulation. Since L-NAME is an inhibitor of NOS, we expected enhanced autoregulation.¹⁹ In SDRs, we see that during L-NAME infusion there is an increase in the MR peak gain that is accompanied by significant AM of the MR by either TGF or a 0.01 Hz component. These results agree with those from Shi *et al.* that show augmentation of the MR during inhibition of NOS¹⁹ and Sosnovtseva *et al.* that show increased modulation after infusion of L-NAME.²⁵ By using analytical methods to detect modulation and track temporal changes in the system gain we are able to identify that changes in the transfer function may be due to changes in the interactions between the MR and TGF. The autoregulation mechanisms are more active after L-NAME,¹⁹ so it stands that the interaction between them should be more pronounced given that they both act on the afferent arteriole. It may also represent a change in TGF regulation over the MR after NOS inhibition. Use of multiple analytical methods allows us to better understand how interactions between the MR and TGF may contribute to the overall effectiveness of renal autoregulation.

Without examining coherence we cannot say if changes in transfer function gain of the CBF oscillations are caused by a linear transformation of the input BP signal, as coherence determines the confidence of the transfer function analysis.¹³ Coherence has been repeatedly studied in renal autoregulation.^{1,3,5,14,19,32} The frequency region >0.1 Hz, containing the MR, has been reported to have high coherence showing that the MR is a direct consequence of changes in BP.^{14,19} Time-invariant coherence is often shown to be low in the TGF frequency range,³ contributing to the concept that TGF can be driven by either non-linear self-sustained oscillations or time-varying dynamics.⁸ Using time-varying approaches directly accounts for the contribution of non-stationarity as we are now able to look at specific time points when time-varying coherence may be high or low and treat the transfer function results appropriately.³ In the present study, we did not examine coherence, and the transfer function gain results should be interpreted with this in mind.

We have compared a number of time-varying analysis methods, and it is clear that a single method with fixed parameters cannot uncover all the complex

characteristics of the MR and TGF. If one is interested in determining modulation of the dynamics over time between the two control systems, it may be best to use a non-parametric method with settings not fixed for the MR and TGF regions but instead set for each as appropriate. Alternatively, a parametric method such as TVOPS might be the most appropriate for accurate estimation of temporal changes in transfer functions to describe how the system alters its response to BP over time.³ In this study, we limited our comparisons to AM and FM phenomena and time-varying changes in system gain, but the same type of quantitative comparisons could be made for additional parameters of interest such as coherence and phase relationships.

ACKNOWLEDGMENTS

This work was supported by Canadian Institutes of Health Research Grant MOP-102694 to WAC, BB, and KHC. CGS was supported by an American Heart Association Predoctoral Fellowship.

REFERENCES

- ¹Bidani, A. K., R. Hacıoglu, I. Abu-Amarah, G. A. Williamson, R. Loutzenhisser, and K. A. Griffin. "Step" vs. "dynamic" autoregulation: implications for susceptibility to hypertensive injury. *Am. J. Physiol. Renal Physiol.* 285:F113–F120, 2003.
- ²Chon, K. H., R. Raghavan, Y.-M. Chen, D. J. Marsh, and K.-P. Yip. Interactions of TGF-dependent and myogenic oscillations in tubular pressure. *Am. J. Physiol. Renal Physiol.* 288:F298–F307, 2005.
- ³Chon, K. H., Y. Zhong, L. C. Moore, N. H. Holstein-Rathlou, and W. A. Cupples. Analysis of nonstationarity in renal autoregulation mechanisms using time-varying transfer and coherence functions. *Am. J. Physiol. Regul. Integr. Comp. Physiol.* 295:R821–R828, 2008.
- ⁴Cupples, W. A. Interactions contributing to kidney blood flow autoregulation. *Curr. Opin. Nephrol. Hypertens.* 16:39–45, 2007. doi:10.1097/MNH.0b013e3280117fc7.
- ⁵Cupples, W. A., and B. Braam. Assessment of renal autoregulation. *Am. J. Physiol. Renal Physiol.* 292:F1105–F1123, 2007.
- ⁶Cupples, W. A., P. Novak, V. Novak, and F. C. Salevsky. Spontaneous blood pressure fluctuations and renal blood flow dynamics. *Am. J. Physiol. Renal Physiol.* 270:F82–F89, 1996.
- ⁷Hlawatsch, F., and G. F. Boudreaux-Bartels. Linear and quadratic time-frequency signal representations. *IEEE Signal Process. Mag.* 9:21–67, 1992.
- ⁸Holstein-Rathlou, N. H., A. J. Wagner, and D. J. Marsh. Tubuloglomerular feedback dynamics and renal blood flow autoregulation in rats. *Am. J. Physiol. Renal Physiol.* 260:F53–F68, 1991.
- ⁹Just, A., and W. J. Arendshorst. Dynamics and contribution of mechanisms mediating renal blood flow autoregulation. *Am. J. Physiol. Regul. Integr. Comp. Physiol.* 285:R619–R631, 2003.
- ¹⁰Marsh, D. J., O. V. Sosnovtseva, A. N. Pavlov, K.-P. Yip, and N.-H. Holstein-Rathlou. Frequency encoding in renal blood flow regulation. *Am. J. Physiol. Regul. Integr. Comp. Physiol.* 288:R1160–R1167, 2005.
- ¹¹Marsh, D. J., I. Toma, O. V. Sosnovtseva, J. Peti-Peterdi, and N.-H. Holstein-Rathlou. Electrotonic vascular signal conduction and nephron synchronization. *Am. J. Physiol. Renal Physiol.* 296:F751–F761, 2009.
- ¹²Pavlov, A. N., O. V. Sosnovtseva, O. N. Pavlova, E. Mosekilde, and N.-H. Holstein-Rathlou. Characterizing multimode interaction in renal autoregulation. *Physiol. Meas.* 29:945, 2008.
- ¹³Pinna, G., and R. Maestri. Reliability of transfer function estimates in cardiovascular variability analysis. *Med. Biol. Eng. Comput.* 39:338–347, 2001.
- ¹⁴Pires, S. L. S., C. Barrès, J. Sassard, and C. Julien. Renal blood flow dynamics and arterial pressure lability in the conscious rat. *Hypertension* 38:147–152, 2001.
- ¹⁵Pittner, J., M. Wolgast, D. Casellas, and A. E. G. Persson. Increased shear stress-released NO and decreased endothelial calcium in rat isolated perfused juxtamedullary nephrons. *Kidney Int.* 67:227–236, 2005.
- ¹⁶Powers, E. J., H. S. Don, J. Y. Hong, Y. C. Kim, G. A. Hallock, and R. L. Hickok. Spectral analysis of non-stationary plasma fluctuation data via digital complex demodulation. *Rev. Sci. Instrum.* 59:1757–1759, 1988.
- ¹⁷Raghavan, R., X. Chen, K.-P. Yip, D. J. Marsh, and K. H. Chon. Interactions between TGF-dependent and myogenic oscillations in tubular pressure and whole kidney blood flow in both SDR and SHR. *Am. J. Physiol. Renal Physiol.* 290:F720–F732, 2006.
- ¹⁸Sheng, L., J. Ki Hwan, and K. H. Chon. A new algorithm for linear and nonlinear ARMA model parameter estimation using affine geometry [and application to blood flow/pressure data]. *IEEE Trans. Biomed. Eng.* 48:1116–1124, 2001.
- ¹⁹Shi, Y., X. Wang, K. H. Chon, and W. A. Cupples. Tubuloglomerular feedback-dependent modulation of renal myogenic autoregulation by nitric oxide. *Am. J. Physiol. Regul. Integr. Comp. Physiol.* 290:R982–R991, 2006.
- ²⁰Siu, K. L., B. Sung, W. A. Cupples, L. C. Moore, and K. H. Chon. Detection of low-frequency oscillations in renal blood flow. *Am. J. Physiol. Renal Physiol.* 297:F155–F162, 2009.
- ²¹Sosnovtseva, O. V., A. N. Pavlov, E. Mosekilde, and N.-H. Holstein-Rathlou. Bimodal oscillations in nephron autoregulation. *Phys. Rev. E* 66:061909, 2002.
- ²²Sosnovtseva, O. V., A. N. Pavlov, E. Mosekilde, N.-H. Holstein-Rathlou, and D. J. Marsh. Double-wavelet approach to study frequency and amplitude modulation in renal autoregulation. *Phys. Rev. E* 70:031915, 2004.
- ²³Sosnovtseva, O. V., A. N. Pavlov, E. Mosekilde, N.-H. Holstein-Rathlou, and D. J. Marsh. Double-wavelet approach to studying the modulation properties of non-stationary multimode dynamics. *Physiol. Meas.* 26:351, 2005.
- ²⁴Sosnovtseva, O. V., A. N. Pavlov, E. Mosekilde, K.-P. Yip, N.-H. Holstein-Rathlou, and D. J. Marsh. Synchronization among mechanisms of renal autoregulation is reduced in hypertensive rats. *Am. J. Physiol. Renal Physiol.* 293:F1545–F1555, 2007.
- ²⁵Sosnovtseva, O. V., A. N. Pavlov, O. N. Pavlova, E. Mosekilde, and N.-H. Holstein-Rathlou. The effect of L-NAME on intra- and inter-nephron synchronization. *Eur. J. Pharm. Sci.* 36:39–50, 2009.

- ²⁶Torrence, C., and G. P. Compo. A practical guide to wavelet analysis. *Bull. Am. Meteorol. Soc.* 79:61–78, 1998.
- ²⁷Wang, X., and W. A. Cupples. Interaction between nitric oxide and renal myogenic autoregulation in normotensive and hypertensive rats. *Can. J. Physiol. Pharmacol.* 79:238–245, 2001.
- ²⁸Wang, H., K. L. Siu, K. Ju, and K. H. Chon. A high resolution approach to estimating time-frequency spectra and their amplitudes. *Ann. Biomed. Eng.* 34:326–338, 2006.
- ²⁹Whitcher, B., P. F. Craigmile, and P. Brown. Time-varying spectral analysis in neurophysiological time series using Hilbert wavelet pairs. *Signal. Process.* 85:2065–2081, 2005.
- ³⁰Yip, K. P., N. H. Holstein-Rathlou, and D. J. Marsh. Mechanisms of temporal variation in single-nephron blood flow in rats. *Am. J. Physiol. Renal Physiol.* 264:F427–F434, 1993.
- ³¹Zhao, H., W. A. Cupples, K. H. Ju, and K. H. Chon. Time-varying causal coherence function and its application to renal blood pressure and blood flow data. *IEEE Trans. Biomed. Eng.* 54:2142–2150, 2007.
- ³²Zhao, H., S. Lu, R. Zou, K. Ju, and K. Chon. Estimation of time-varying coherence function using time-varying transfer functions. *Ann. Biomed. Eng.* 33:1582–1594, 2005.
- ³³Zou, R., W. A. Cupples, K. R. Yip, N. H. Holstein-Rathlou, and K. H. Chon. Time-varying properties of renal autoregulatory mechanisms. *IEEE Trans. Biomed. Eng.* 49:1112–1120, 2002.
- ³⁴Zou, R., H. Wang, and K. H. Chon. A robust time-varying identification algorithm using basis functions. *Ann. Biomed. Eng.* 31:840–853, 2003.